Polyhedron 149 (2018) 109–116

Contents lists available at ScienceDirect

Polyhedron

journal homepage: www.elsevier.com/locate/poly

A new molecular switch based on a symmetrical dinuclear complex of two tricarbonylrhenium(I) moieties bridged by 4,4″-azobis-(2,2′-bipyridine)

Pedro O. Abate [a], Gaston Pourrieux [a], Faustino E. Morán Vieyra [b], Mauricio Cattaneo [a], Mónica M. Vergara [a], Néstor E. Katz [a,*]

[a] INQUINOA-UNT-CONICET, Instituto de Química Física, Facultad de Bioquímica, Química y Farmacia, Universidad Nacional de Tucumán, Ayacucho 471, T4000INI San Miguel de Tucumán, Argentina
[b] INBIONATEC-UNSE-CONICET, Universidad Nacional de Santiago del Estero, RN9, Km 1125 (G4206XCP), Santiago del Estero, Argentina

ARTICLE INFO

Article history:
Received 14 December 2017
Accepted 20 April 2018
Available online 30 April 2018

Keywords:
Rhenium carbonyls
Azobipyridines
L-Cysteine sensing
Molecular switches
Proton-coupled electron transfer

ABSTRACT

A new symmetrical dinuclear complex of two tricarbonylrhenium(I) moieties, of formula $[(CH_3CN)(CO)_3Re(4,4''\text{-azobpy})\ Re(CO)_3(CH_3CN)](PF_6)_2$, with 4,4″-azobpy = 4,4″-azobis-(2,2′-bipyridine), has been synthesized and characterized by spectroscopic, electrochemical, spectroelectrochemical, photophysical and computational techniques. The bridging azo group in the bipyridyl ring decreases the emission quantum yield of the ^{3}MLCT lowest-lying excited state respect to similar Re(I) complexes and introduces a new emissive excited state with a longer lifetime, due to increased electronic delocalization in the bridging ligand. When reducing the azo group in CH_3CN/H_2O mixtures with sodium dithionite, the emission is enhanced by an order of magnitude. Therefore, this complex can be used as a "molecular switch" with electron and proton additions. Besides, changes in the absorption spectrum on addition of L-Cysteine can be applied for sensing aminoacids with reducing thiol groups. The electronic structures calculated by DFT methods agree reasonably well with experimental results.

1. Introduction

Tricarbonylrhenium(I) moieties coordinated to diimine ligands such as 2,2′-bipyridine and derivatives have been extensively studied due to their interesting photophysical properties, such as photostability and long-lived excited states, which have led to multiple applications; for example, in designing new sensors [1] or new solar energy conversion schemes [2].

The azo functionality (—N=N—) in pyridyl ligands introduces the possibility of developing new molecular "switches", i.e. materials with optical properties that change considerably upon addition of protons, electrons or photons [3]. For example, we have previously reported a tricarbonyl(2,2′-bipyridine)rhenium(I) complex with the monodentate ligand 4,4′-azpy (4,4′-azpy = 4,4′-azobis(pyridine)) and found that this compound is almost non-emissive at room temperature but recovers luminescence by an order of magnitude either by reduction of coordinated 4,4′-azpy or by *trans*- to *cis*-photoisomerization of 4,4′-azpy, thus pointing to its possible applications as components of logic circuits at the molecular scale [4].

Exhaustive studies by Otsuki et al. have disclosed considerable absorption and emission changes triggered by electron transfer in Ru and Os bipyridyl multinuclear complexes containing the azo group in the bidentate ligand 4,4″-azobpy or 4,4″-azobis(2,2′-bipyridine) [5].

Taking all these previous studies into account, we thought that introducing the 4,4″-azobpy as a bridging ligand in the coordination sphere of two rhenium(I)tricarbonyls with no other chromophoric species competing for the electron density of the metallic center would give rise to a new species with interesting properties that can be used for sensing purposes. For example, detecting L-Cysteine is an important issue considering that abnormal levels of thiols in human blood can be an indication of different metabolic and mental disorders [6]. With that motivation, we describe in this work a new complex with L = 4,4″-azobpy acting as a bridge in a symmetrical dinuclear species of Re(I), of formula $[\{Re(CO)_3(CH_3CN)\}_2(\mu\text{-L})](PF_6)_2$, (**1**)$(PF_6)_2$, whose structure is shown in Scheme 1.

* Corresponding author.
E-mail address: nkatz@fbqf.unt.edu.ar (N.E. Katz).

https://doi.org/10.1016/j.poly.2018.04.029
0277-5387/

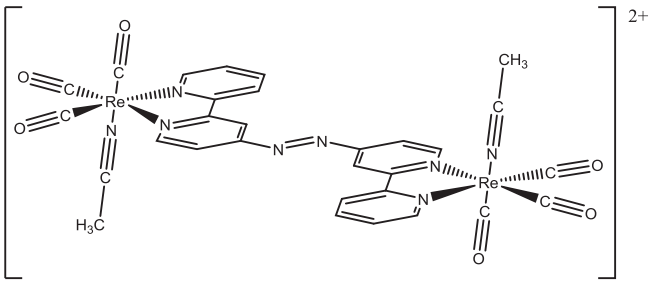

Scheme 1. Structure of complex (**1**).

2. Experimental

2.1. Materials and techniques

All chemicals used in this work were analytical-reagent grade. The commercially available compounds $[Re(CO)_5Cl]$, $Ag(CF_3SO_3)$, $Na_2S_2O_4$ and L-Cysteine were used as received. CH_3CN was freshly distilled over P_4O_{10} for electrochemical measurements. Tetrakis(*n*-butyl)ammoniumhexafluorophosphate (TBAH) was dried at 150 °C for 24 h before being used as supporting electrolyte in electrochemical measurements. UV–Vis spectra were recorded on a Varian Cary 50 spectrophotometer, using 1-cm quartz cells. IR spectra were obtained as KBr pellets with a Perkin–Elmer Spectrum RX-I FTIR spectrometer. Emission measurements were carried out in 1-cm fluorescence cells with a Shimadzu RF-5301 PC spectrofluorometer. The optical density of the solutions at the excitation wavelength was below 0.1 to minimize both inner filtering and re-absorption effects. The fluorescence quantum yields (Φ_F) in Ar saturated solutions were determined using $Ru(bpy)_3^{2+}$ in CH_3CN as actinometer ($\Phi_F = 0.062$) [7], by comparing the integrated fluorescence intensity of the sample and reference solutions as described elsewhere [8]. This used actinometer is the usual one for determining values of quantum yields in tricarbonyl Re(I) complexes [9]. Fluorescence decays were obtained with a Tempro-01 TCSPC (Time Correlated Single Photon Counting) apparatus of Horiba Jobin Yvon, using as excitation pulse source an ultrafast Nanoled® at 340 and 390 (±15) nm, operating at 1 MHz. The emission wavelengths were selected at 500, 540 and 580 nm with a monochromator with emission bandwidth selected at 12 nm. All measurements were performed at room temperature and under Ar-saturated conditions. The fluorescence intensity decay was fitted with the Fluorescence Decay Analysis Software DAS6® of Horiba Jobin Yvon by deconvolution of the pulse function using the multi-exponential model function:

$$I_{(t)} = \sum_{i=1}^{n} \alpha_i exp(-t/\tau_i) \quad (1)$$

where n is the number of single exponential decays, τ_i and α_i are the decay time and the fluorescence intensity amplitude at $t = 0$ of each decay, respectively. Cyclic voltammetry (CV) and differential pulse voltammetry (DPV) experiments were carried out using BAS Epsilon EC equipment, with vitreous C as working electrode, Pt wire as auxiliary electrode, and a Ag/AgCl (3 M NaCl) reference electrode. The cyclic voltammograms were measured at a scan rate of 100 mV/s unless otherwise noted. The solutions used in voltammetry were degassed with Ar prior to each measurement. The IR OTTLE cell was equipped with CaF_2 windows, a Pt-minigrid as working electrode, a Pt-minigrid as auxiliary electrode and a Ag wire pseudo-reference electrode [10]. Controlled potential electrolyses within the OTTLE cell were carried out using a Teq-04 potentiostat. Spectroelectrochemical measurements in the UV–Vis region were performed by using a Honeycomb Cell from PINE Research Instrumentation, equipped with a Pt working electrode, a Pt counter electrode and a Ag/AgCl (saturated KCl) reference electrode. Controlled potential electrolyses with this cell were carried out using the BAS potentiostat. NMR spectra were obtained in CD_3CN with a Bruker 200 MHz equipment. Chemical analyses were performed at INQUIMAE, University of Buenos Aires, Buenos Aires, Argentina, with an estimated error of ±0.5%. TD-DFT calculations were carried out with GAUSSIAN-03 program package [11]. Molecular structures of all species were optimized using the Becke's three-parameter hybrid functional B3LYP [12], with the local term of Lee, Yang, and Parr [13]. The basis set LanL2DZ was chosen for all atoms. To include solvent polarization effects, all the calculations were done by using the conductor-like polarizable continuum model (CPCM) with CH_3CN as solvent. The contribution of different groups on the orbitals and partial density of states (PDOS) calculations were determined with the GAUSSSUM Version 2.2 Program [14].

2.2. Synthesis of *L = 4,4″-azobpy*

The ligand 4,4″-azobis-(2,2′-bipyridine) was synthesized by reductive coupling of 4-nitro-(2,2′-bipyridine) following previously reported methods [15] with small modifications, consisting in the extension of the heating time (6 h) and activation of Zn dust by treating it with 3 M HCl for 20 min.

2.3. Synthesis of *[{Re(CO)$_3$(Cl)}$_2$(μ-L)]·2.5H$_2$O*

65.6 mg (0.194 mmol) of 4,4″-azobpy were dissolved in $CHCl_3$ (52 mL), together with 140.2 mg (0.388 mmol) of $[Re(CO)_5Cl]$ and then 39 mL of CH_3OH were added. After heating at reflux and stirring for 6 h, the solution changed from an orange to a reddish color. Upon cooling to r.t., the reaction mixture was kept at −20 °C for one hour and a red precipitate was observed. The formed solid was isolated by suction filtration with a glass filter and washed with $CHCl_3$ (3 × 15 mL) and diethyl ether (2 × 10 mL). The obtained red solid was dried under vacuum over P_4O_{10} for 24 h. Yield: 131.6 mg (71.4%). *Anal.* Calc. for $Re_2C_{26}N_6H_{19}Cl_2O_{8.5}$: C, 31.4; N, 8.4; H, 1.9. Found: C, 31.7; N, 8.6; H, 1.7%. NMR spectra in CH_3CN could not be obtained due to its insolubility.

2.4. Synthesis of *[{Re(CO)$_3$(CH$_3$CN)}$_2$((μ-L)](PF$_6$)$_2$·0.5H$_2$O*

This complex was prepared by heating 83.7 mg (0.088 mmol) of [{$Re(CO)_3(Cl)$}$_2$(4,4″-azobpy)] with 49.8 mg (0.194 mmol) of $Ag(CF_3SO_3)$ under reflux in a 30 mL mixture of CH_3CN/1,4-Dioxane (v/v, 1/2) during 10 h. Upon cooling to r.t., the mixture was kept at −5 °C for 30 min and the precipitated AgCl was filtrated. After 24 hs at −20 °C the filtrate from the first filtration was filtrated once again to eliminate the remaining AgCl and the solution was rotoevaporated to 1 mL; then, 5 mL of CH_3CN were added and the remaining solution was poured on a saturated NH_4PF_6 aqueous solution. The mixture was kept at 5 °C for four days. The formed solid was filtered, washed with H_2O (3 × 10 mL) and diethyl ether (2 × 10 mL). The obtained orange solid was dried under vacuum over P_4O_{10} for 24 h. Yield: 75.2 mg (68.4%). *Anal.* Calc. for $Re_2C_{30}N_8O_6H_{20}P_2F_{12}·0.5H_2O$: C, 28.6; N, 8.9; H, 1.7. Found: C, 29.0; N, 9.1; H, 1.7%. ^{1}H NMR (200 MHz, CD_3CN) 9.33 (dd, 1H), 9.12 (ddd, 1H), 8.96 (d, 1H), 8.69 (dt, 1H), 8.40 (td, 1H), 8.13 (dd, 1H), 7.83 (ddd, 1H). ^{13}C NMR (50 MHz, CD_3CN) δ = 159.8, 159.5, 157.3, 156.5, 155.2, 142.1, 129.8, 125.9, 120.6, 118.9, 123.3, 3.9. ^{15}N NMR (20.26 MHz, CD_3CN) δ = 533.5, 243.8, 237.4, 173.

3. Results and discussion

3.1. Syntheses

The used synthetic procedures were similar to those previously described for related tricarbonylpolypyridyl-rhenium(I) complexes [16,17]. The precursor chloro-containing species was insoluble in water or organic solvents, so that only the IR spectrum of the solid was obtained, as reported below. The new complex was soluble in organic solvents and its purity was confirmed by chemical analyses, IR and NMR spectra.

3.2. IR and NMR spectra

As shown in Fig. 1, the IR spectrum of (**1**)$(PF_6)_2$ contains three bands at 2039, 1922 and 1912 cm^{-1}, corresponding to ν(C≡O), the carbonyl stretching modes of A′(1), A″ and A′(2) symmetries respectively, being characteristic of Re(I) tricarbonyl complexes with a facial configuration [18]. The bands at 1922 and 1912 cm^{-1} were obtained by Lorentzian deconvolution, since it is well known that in complexes of the type $[Re(N^N)(CO)_3X]^+$ (with N^N = bidentate diimine ligand, X = acceptor ligand), these two bands may appear as a broad band due to a quasi-degeneracy of the A″ and A′(2) modes [19]. These wavenumber values are blue-shifted respect to those corresponding to the precursor chloro-complex mentioned above (ν(C≡O = 2023, 1916 and 1902 cm^{-1}), due to the increased charge of this complex [20].

The chemical shifts of ^1H, ^{13}C and ^{15}N for (**1**) in CD_3CN are shown in the Section 2. Signal assignments could be accomplished by using bidimensional techniques, such as COSY, ^{13}C HSQC, ^{13}C HMBC and ^{15}N HMBC. Due to the symmetric structure of complex (**1**), its ^1H NMR spectrum displays 7 groups of aromatic signals between 7.7 and 9.4 ppm, as shown in Fig. 2. This number is the same to that corresponding to the H atoms of the 4,4″-azobpy free ligand; upon coordination to the metallic center, a deshielding effect is disclosed. A structure of the complex with the proton numbering scheme is shown above Fig. 2. The signals of the coordinated CH_3CN ligands are shifted to lower fields as compared to those of free CH_3CN, due to the inductive effect of the metallic center.

3.3. UV–Vis spectrum

The UV–Vis spectrum of (**1**) in CH_3CN is shown in Fig. 3. The bands observed below 300 nm can be assigned to IL transitions of 4,4″-azobpy, by comparison with those observed for the free ligand in CH_3CN (λ_{max} = 242 and 284 nm). The broad band between 300 nm and 500 nm was deconvoluted into two components, which can be assigned to MLCT $d_\pi(Re) \rightarrow \pi^*$(4,4″-azobpy) transitions. The band at lowest energy (λ_{max} = 400 nm) can be attributed to an electron promotion from the HOMO – mainly localized in the metal- to the LUMO – mainly localized in the azo bridge –. On the other hand, the higher energy band (λ_{max} = 346 nm) can be attributed to a transition from the HOMO to the LUMO + 1 – mainly localized in the bipyridyl rings –. These assignments are confirmed by TD-DFT calculations, as shown below in the corresponding Section and by comparison to the maximum of the lowest-energy MLCT d_π (Re) → π^*(bpy) band in the $[Re(bpy)(CO)_3(CH_3CN)]^+$ complex (λ_{max} = 360 nm in CH_3CN, [20]); the shift to lower energies in (**1**) can be accounted for by the greater π-electron delocalization induced by 4,4″-azobpy acting as a bridging ligand.

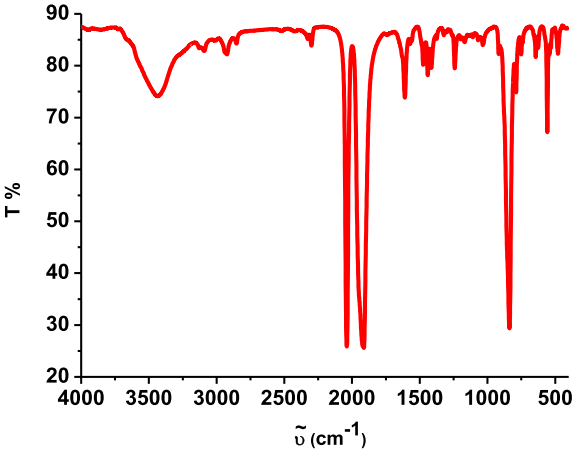

Fig. 1. IR spectrum of (**1**) $(PF_6)_2$ (as KBr pellet).

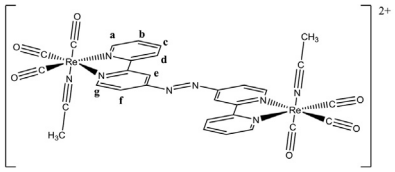

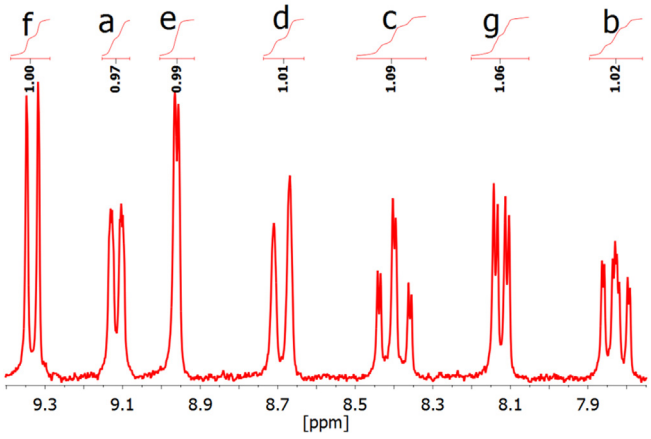

Fig. 2. ^1H NMR spectrum of complex (**1**), in CD_3CN.

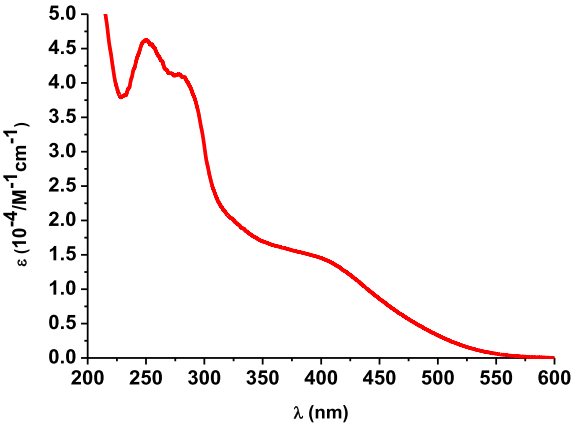

Fig. 3. UV–Vis spectrum of (**1**), in CH_3CN.

3.4. Electrochemistry

In order to study the redox properties of (**1**), cyclic voltammetry (CV) and differential pulse voltammetry (DPV) were carried out in

CH_3CN with 0.1 M TBAH. The obtained $E_{1/2}$ values are referred to Ag/AgCl. As shown in Fig. 4, in the oxidative region, the Re^{II}/Re^{I} couple exhibits a value of $E_{1/2}$ = 1.87 V, which is similar to those reported for similar complexes [21]. As shown in Fig. 5(a), in the reductive region, the reversible wave at $E_{1/2}$ = −0.12 V and the quasi-reversible wave at $E_{1/2}$ = −0.50 V can be attributed to the first and the second one-electron reduction processes located at the azo bridge [22,23] respectively. The quasi-reversibility of the second wave can be attributed to a chemical reaction at the electrode, similar to that observed in the electrochemical second reduction of 4,4′-azopyridine [24]. The reductive processes at $E_{1/2}$ = −1.49 V, −1.64 V and −1.96 V, shown in Fig. 5(b), can be assigned to the redox couples bpy^0/bpy^-, Re^I/Re^0 and bpy^-/bpy^{2-} respectively, by comparison to similar species [17].

3.5. UV–Vis spectroelectrochemistry

As shown in Fig. 6, when an external potential E = −316 mV is applied in a spectroelectrochemical cell to a solution of **(1)** in CH_3CN ($C \sim 10^{-4}$ M), a decrease in the intensity of the IL transitions bands is observed, and new bands appear at λ_{max} = 460, 550 and 800 nm which can be attributed to IL transitions of the azobpy$^{\cdot-}$ radical as expected after one-electron reduction of (**1**) : these bands are similar to those reported for reduced azo compounds [4,23]. The MLCT band at λ_{max} = 400 nm is shifted to higher energies, which can be explained by the increase of electron density in the bridging ligand upon reduction and the subsequent destabilization of the Re (d_π) orbitals. When the applied potential is restored to 0 V, the original spectrum is fully recovered, in consistency with the reversibility observed in CV for the first reductive process of L (see Fig. 5(a)). As shown in Fig. 7, when an external potential E = −800 mV is applied, the intensities of the bands attributed to the radical increase when compared to those of the first one-electron reduction and the MLCT band shifts to even higher energies. The UV–Vis spectra of the two-electron reduction processes could be separated in two set of spectra: the first one corresponded to the first one-electron reduction with an isosbestic point at λ = 395 nm and the second one to the subsequent two-electron reduction with two isosbestic points at λ = 449 nm and 595 nm.

3.6. FTIR spectroelectrochemistry

As shown in Fig. 8, by using an IR spectroelectrochemical cell with an applied external potential E = −316 mV, the frequencies corresponding to ν(C≡O) are shifted to lower energies, with isosbestic points at 2036 and 1932 cm^{-1}, the band assigned to the CO_{eq}

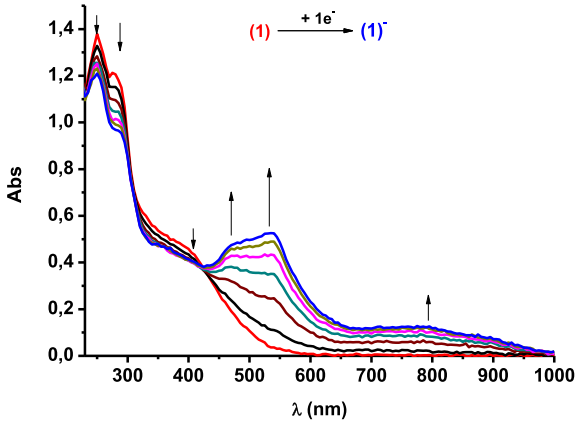

Fig. 6. UV–Vis absorption changes of (**1**) in CH_3CN after applying an external potential E = −316 mV.

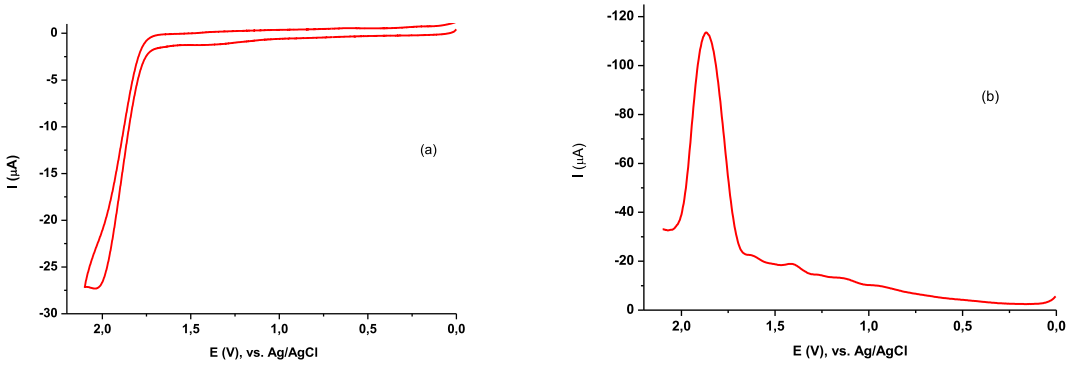

Fig. 4. (a) CV and (b) DPV in the oxidative region of complex (**1**) in CH_3CN, 0.1 M TBAH.

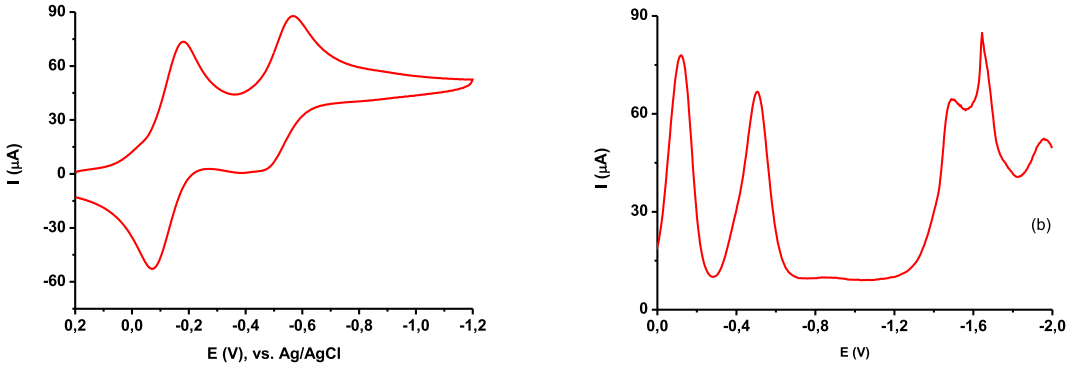

Fig. 5. (a) CV and (b) DPV in the reductive region of complex (**1**) in CH_3CN, 0.1 M TBAH.

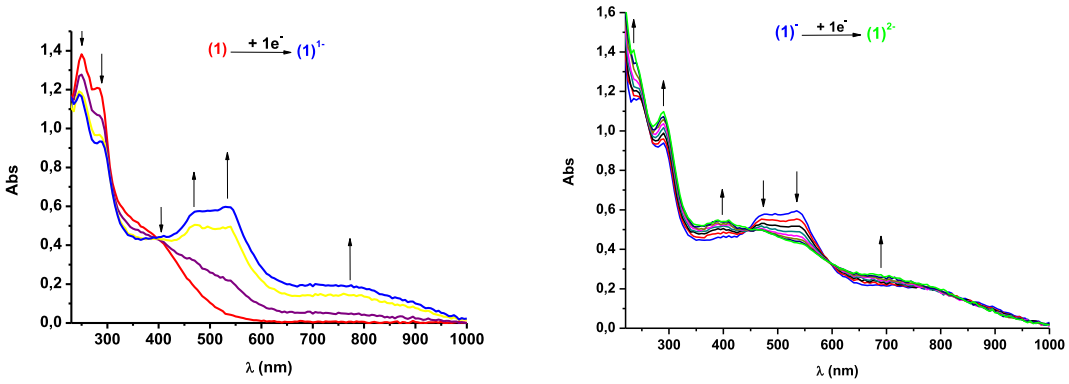

Fig. 7. UV–Vis absorption changes of (**1**) in CH_3CN after applying an external potential $E = -800$ mV separated in two subsequent one-electron processes.

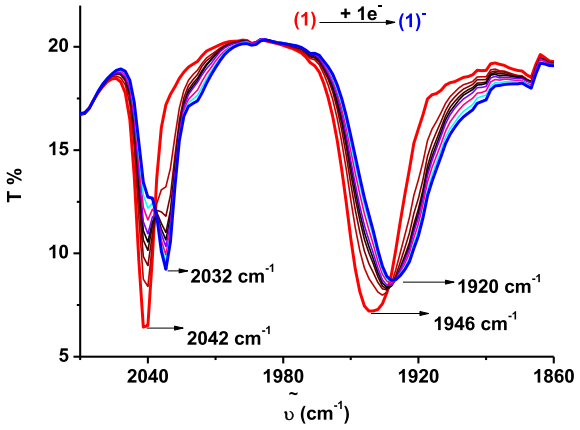

Fig. 8. IR changes upon reduction of (**1**) in CH_3CN, at $E = -316$ mV.

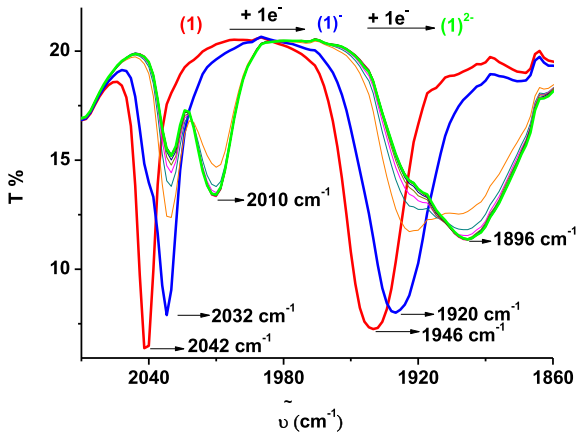

Fig. 9. IR changes upon reduction of (**1**) in CH_3CN at $E = -770$ mV.

being more affected. This effect can be explained by considering that the electron withdrawing character of 4,4″-azobpy is diminished when its electron density increases upon reduction, thus leading to an increase of the π-backbonding effect from the metallic center to the CO ligands and a consequent decrease of the CO bond orders. The frequencies of the CO_{eq} groups are more affected since they have the adequate symmetry to interact with the metal orbitals, in contrast to the CO_{ax} groups that are orthogonal to the 4,4″-azobpy ligand [25,26]. When the applied potential is restored to 0 V, the original spectrum is fully recovered.

As shown in Fig. 9, when an external potential $E = -770$ mV is applied, a more pronounced shift to lower energies of the CO bands is observed, as expected after a two-electron reduction process of L. Isosbestic points are also detected and the spectrum of the one-electron reduction product is observed at the beginning of the process.

3.7. Chemical reductions

Reduction with L-Cysteine: The UV–Vis spectral changes of (**1**) ($C \sim 2 \times 10^{-5}$ M) upon addition of the reductant L-Cysteine were measured in a mixture H_2O/CH_3CN (v/v, 1/1) at pH 6 and are shown in Fig. 10(a). After the addition of each aliquot of L-Cysteine (under Ar) to a bulk solution of (**1**), the solution was kept under stirring for 5 min and the UV–Vis spectrum was measured. After reduction, the LUMO is populated and the band at $\lambda_{max} = 400$ nm – assigned to the MLCT of lowest energy – disappears and a new MLCT band at lower energy is observed ($\lambda_{max} = 342$ nm). On the other hand, the new band that appears at $\lambda_{max} = 312$ nm can be assigned to a MLCT from the HOMO to the LUMO+1 (Scheme 2). Above [L-Cys]/[C] = 2/1, no changes in the UV–Vis spectra were detected, thus pointing to a double reduction of the azo group. This chemical reduction is also reversible when the solution is exposed to atmospheric oxygen; after 24 h the spectrum of (**1**) is fully recovered. No changes in the emission spectra were detected. A calibration curve is shown in Fig. 10(b). The detection limit was determined to be in the submicromolar range; complex (**1**) can thus be used as a probe for L-Cysteine sensing.

Reduction with $Na_2S_2O_4$ when an excess of sodium dithionite is added to a solution of (**1**) ($C \sim 10^{-5}$ M) in a mixture CH_3CN/H_2O (v/v, 300/1), the UV–Vis spectrum, as shown in Fig. 11, displays the same changes than those observed upon reduction with L-Cysteine. However, after reduction with dithionite, the emission intensity is enhanced by an order of magnitude in comparison with the non-reduced complex, as shown in Fig. 12. A possible explanation for this emission enhancement effect, which is absent in the L-Cysteine reduced product, is based on the fact that the concentration of water is much higher in the former case and water may quench the emission from the ^{3}MLCT excited state by protonation of the H of the reduced azo moiety. The mechanism for reduction of azo-based compounds [23,27] is already known; we propose in this case a similar reaction sequence. The reason for using different CH_3CN/H_2O ratios in both experiments was the greater insolubility of L-cysteine in CH_3CN. We tested in the case of dithionite that emission is also quenched when increasing the water concentration, supporting the hypothesis that double protonation of the azo group is the origin of the quenching effect. We thus conclude that upon reduction of the azo group at low water concentrations, complex (**1**) behaves as a molecular "switch" of the "off–on" type.

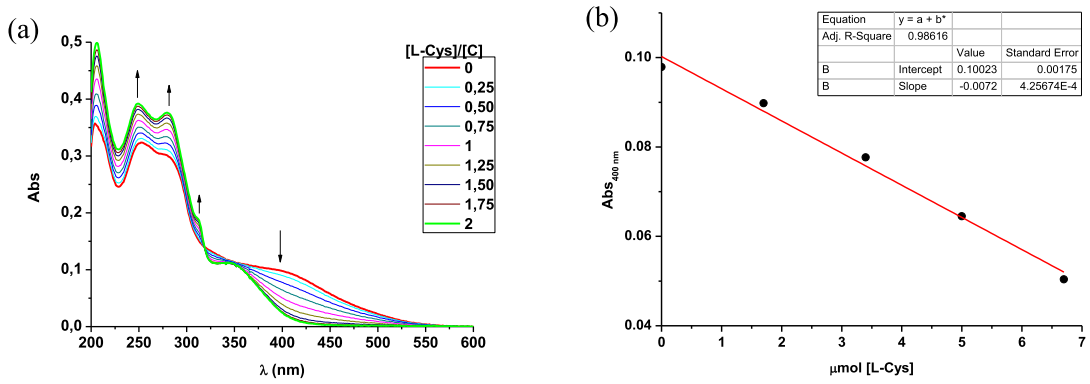

Fig. 10. (a) Addition of varying amounts of L-Cysteine to a solution of (**1**) in H_2O/CH_3CN (v/v, 1/1). (b) Calibration curve for the detection of L-Cysteine at [1] = 6.7 μM and λ_{max} = 400 nm, in H_2O/CH_3CN (v/v, 1/1).

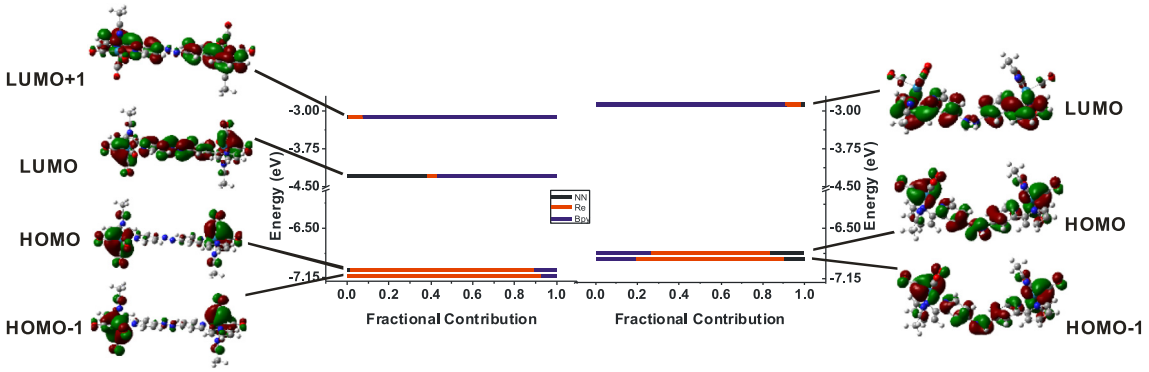

Scheme 2. MO energy diagrams for complex (**1**) at the left and for the doubly reduced and protonated species (**1H₂**) at the right.

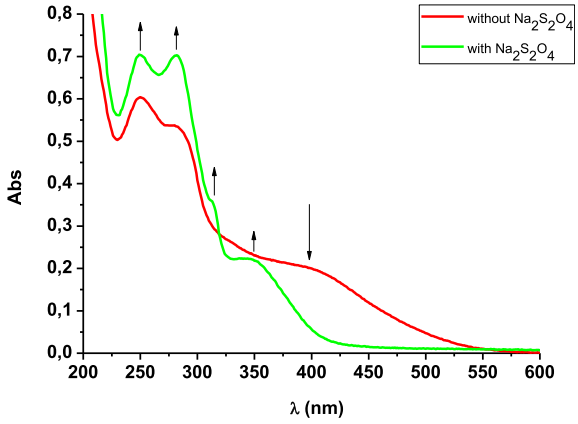

Fig. 11. Red line: UV–Vis spectrum of (**1**). Green line: UV–Vis spectrum of reduced (**1**) upon addition of excess $Na_2S_2O_4$. Both spectra in CH_3CN/H_2O (v/v, 300/1). (Color online.)

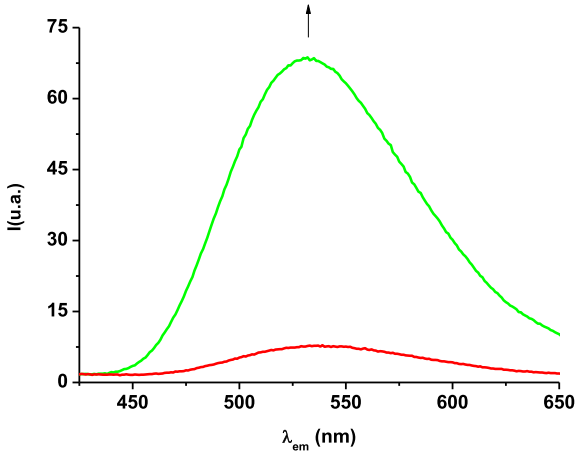

Fig. 12. Red Line: emission spectrum of (**1**). Green line: emission spectrum of reduced (**1**) upon addition of excess $Na_2S_2O_4$. Both spectra in CH_3CN/H_2O (v/v, 300/1), at λ_{ex} = 346 nm. (Color online.)

3.8. Photophysical properties

As shown in Fig. 13, dual emission can be detected for complex (**1**) in pure CH_3CN. At λ_{exc} = 346 nm, a weak emission is observed at λ_{em} = 530 nm (with quantum yield $\phi = 3 \times 10^{-4}$) and this is typical of a decay from a ^{3}MLCT d_π(Re)-π^* excited state with the π^* orbitals centered at the bipyridyl rings [28]; while at λ_{exc} = 400 nm, a new emission appears at λ_{em} = 575 nm (with a similar quantum yield), which can be ascribed to a decay from a ^{3}MLCT d_π(Re)-π^* excited state with the π^* orbitals centered at the azo bridging group. At room temperature, emission bands of tricarbonylpolypyridylrhenium(I) complexes are normally non-structured [28], so we consider that this dual emission cannot be adscribed to coupling to vibrational modes. Although azopyridines usually undergo *cis–trans* isomerization when applying UV–Vis light [4], we irradiated samples of complex (**1**) in CH_3CN solution at λ_{exc} = 270 nm for a couple of hours and no changes in absorption or emission spectra were detected, in agreement with previous reports on Ru complexes with 4,4″-azobpy [22]. This result put into

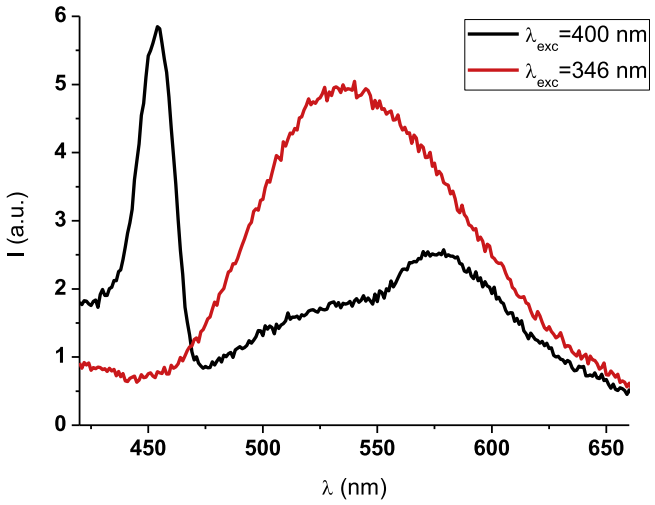

Fig. 13. Emission spectra of (**1**) in deareated CH_3CN, at room temperature and at two excitation wavelengths (the red line corresponds to λ_{exc} = 346 nm and the black line to λ_{exc} = 400 nm). The band at λ_{em} = 450 nm is a Raman band of CH_3CN. (Color online.)

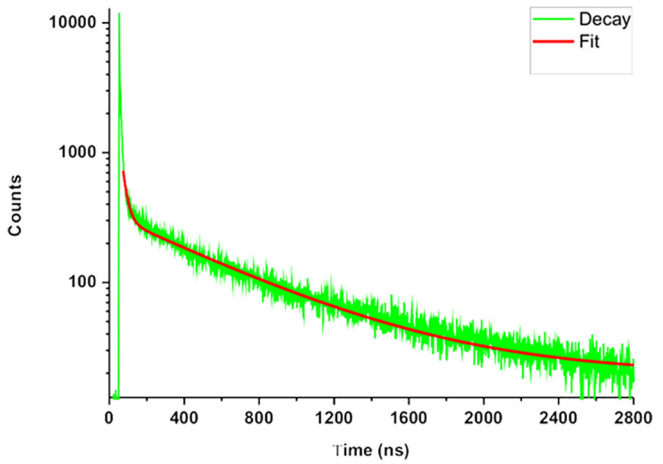

Fig. 14. TCSPC decays of excited states of (**1**) in deareated CH_3CN, at room temperature and λ_{exc} = 390 nm.

evidence that isomerization cannot account for the two nearly isoenergonic emissions.

It is to be noted that this is the first report that reveals emission in complexes containing 4,4″-azobpy as the only chromophoric ligand. In Ru or Os bipyridyl species of 4,4″-azobpy, this luminescence is masked by the strong emission originated from ^{3}MLCT d_π(M)-π^* excited states (M = Ru or Os) with the π^* orbitals centered at the auxiliary 2,2′-bipyridyl ligands [29]. Fig. 14 shows the fit of both decays as measured by TCSPC with two lifetimes: τ = (16 ± 1) ns for the decay at λ_{em} = 530 nm and τ = (621 ± 7) ns for the decay at λ_{em} = 575 nm. The excitation wavelength (λ_{exc} = 390 nm) was close to the value of the absorption maximum of the lowest energy MLCT. The results were similar when using an excitation wavelength (λ_{exc} = 340 nm) close to the value of the higher energy MLCT, but the weighting factor of the lower lifetime is much higher, as shown in Suppl. Table 1, supporting its assignment to the emission at λ_{em} = 530 nm.

Both the quantum yield and the lifetime for the first decay are much lower than those reported for similar Re(I) species [28], indicating luminescence quenching by crossing to the second MLCT state, which in turn decays with a low quantum yield due to quenching by excited states of the bridging ligand; the longer lifetime may be due to increased delocalization on the bridging ligand 4,4″-azobpy as compared to bpy. It is well known that lifetimes of excited states of this type of complexes can be deeply enhanced when IL transitions are involved [28,30]. Additional evidence that the lowest-energy emission is originated from an excited state with the LUMO centered on the azo moiety comes from TD-DFT calculations, as described in the following paragraph.

3.9. TD-DFT calculations

TD-DFT calculations were done as described in the Experimental Section for both complex (**1**) and its reduced and protonated form (hydrazine bridge). Scheme 2 shows the energy level diagrams together with figures for some frontier MO's. The LUMO for complex (**1**) is centered on the azo moiety of 4,4″-azobpy, while that of the reduced and protonated species (**1H$_2$**) is centered on the bipyridyl rings of 4,4″-azobpy. These findings are consistent with the spectroscopic and photophysical properties described before. Although dual emission can be detected from both excited states, as shown in the above paragraph, the quantum yields are very low. However, when a strong reductant such as dithionite is added in acetonitrile/water (v/v, 300/1), the emission is enhanced by one order of magnitude (see Fig. 12), as expected when the LUMO becomes centered on the bipyridyl rings. Triplet calculations with TD-DFT calculations did not converge for complex (**1**), so that we cannot verify that the dual emission is due to the difference between two ^{3}MLCT states lying close in energy. However, the excitation spectra shown in Supplementary Fig. 1, clearly indicate that the emission at λ_{em} = 530 nm is due to a chromophoric group absorbing at λ_{max} = 350 nm, while the emission at λ_{em} = 575 nm is due to chromophoric group absorbing at λ_{max} = 400 nm. On the other hand, the Stokes shift of the emission at λ_{em} = 530 nm ($\Delta\delta$ = 1.24 eV) is higher than the Stokes shift of the emission at λ_{em} = 575 nm ($\Delta\delta$ = 0.94 eV), as expected when considering that the aromaticity of the bipyridyl rings is higher than that of the azo group [31]. The difference between both Stokes shifts is then: $\Delta(\Delta\delta)$ = 0.3 eV, a value which is close to the difference between the energies of both emission bands (ΔE = 0.2 eV), thus supporting the explanation that the emission bands come from nearly isoenergetic ^{3}MLCT excited states.

Additionally, the MO energy diagrams in Scheme 2 indicate that the difference between the LUMO and the HOMO of the reduced/protonated form is almost equal to the difference between the LUMO+1 and the HOMO of complex (**1**), so that both emissions (originated from a MLCT excited state centered on the bipyridyl rings) are expected to occur at almost the same energies.

4. Conclusions

A new dinuclear Re(I) complex with 4,4″-azobpy as a bridging ligand, (**1**), has been synthesized as a PF_6^- salt, and was fully characterized by analytical, spectroscopic, electrochemical and photophysical techniques. The spectroscopic (UV–Vis, IR and emission) changes under chemical and electrochemical reduction were studied in order to use (**1**) as a redox probe for the detection of biological relevant thiols. Besides, emission from an excited state with the LUMO centered on the azo moiety of the 4,4″-azobpy ligand was detected for the first time. After reaction with a strong reducing agent such as dithionite in CH_3CN/H_2O (v/v, 300/1) mixtures, emission from the ^{3}MLCT excited states with the LUMO centered on the bipyridyl rings was recovered, thus pointing to its application as a molecular "switch". Quantum mechanical calculations give support for these experimental findings.

Acknowledgements

We thank Consejo Nacional de Investigaciones Científicas y Técnicas (CONICET) from Argentina for financial support (grant PIP-2015-098). P.O.A. thanks CONICET for a graduate fellowship. M.C., F.E.M.V. and N.E.K. are Members of the Research Career (CONICET).

Appendix A. Supplementary data

Supplementary data associated with this article can be found, in the online version, at https://doi.org/10.1016/j.poly.2018.04.029.

References

[1] K.-C. Chang, S.-S. Sun, M.O. Odago, A. Lees, Coord. Chem. Rev. 284 (2015) 111.
[2] J. Rocahova, O. Ishitani, J. Chem. Soc., Dalton Trans. 46 (2017) 8899.
[3] A. Bianchi, E. Delgado-Pinar, E. García-España, C. Giorgi, F. Pina, Coord. Chem. Rev. 260 (2014) 156.
[4] G. Pourrieux, F. Fagalde, I. Romero, X. Fontrodona, T. Parella, N.E. Katz, Inorg. Chem. 49 (2010) 4084.
[5] J. Otsuki, J. Res. Inst. Sci. Tech. Nihon Univ. No. 124 (2011) 26, and references therein.
[6] D. Maheshwaran, S. Priyanga, R. Mayilmurugan, J. Chem. Soc., Dalton Trans. 46 (2017) 11408.
[7] A. Juris, V. Balzani, F. Barigelletti, S. Campagna, P. Belser, A. Von Zelewsky, Coord. Chem. Rev. 84 (1988) 85.
[8] J.R. Lakowicz, Principles of Fluorescence Spectroscopy, 3rd. ed., Springer, Singapore, 2006.
[9] L.A. Sacksteder, A.P. Zipp, E.A. Brown, J. Streitch, J.N. Demas, B.A. DeGraff, Inorg. Chem. 29 (1990) 4335.
[10] M. Krejčik, M. Daněk, F. Hartl, J. Electroanal. Chem. 317 (1991) 179.
[11] M. J. Frisch et al. Gaussian 03, Re C.02; Gaussian Inc., Wallinford, CT, (2004).
[12] A.D.J. Becke, J. Chem. Phys. 98 (1993) 5648.
[13] C. Lee, W. Yang, R.G. Parr, Phys. Rev. B 37 (1988) 785.
[14] N.M. O'Boyle, A.L. Tenderholt, K.M. Langner Available from: J. Comput. Chem. 29 (2008) 839. http://gausssum.sf.net.
[15] J. Otsuki, A. Imai, K. Sato, D.-M. Li, M. Hosoda, M. Owa, T. Akasaka, I. Yoshikawa, K. Araki, T. Suenobu, S. Fukuzumi, Chem. Eur. J. 14 (2008) 2709.
[16] M. Cattaneo, F. Fagalde, N.E. Katz, Inorg. Chem. 45 (2006) 6884.
[17] M. Cattaneo, M.M. Vergara, M.E. García Posse, F. Fagalde, T. Parella, N.E. Katz, Polyhedron 70 (2014) 20–28.
[18] L.A. Worl, R. Duesing, P. Chen, L. Della Ciana, T.J. Meyer, J. Chem. Soc., Dalton Trans. (1991) 849.
[19] A. Vlček, Top. Organomet. Chem. 29 (2010) 73.
[20] T.A. Perkins, W. Humer, T.L. Netzel, K.S. Schanze, J. Phys. Chem. 94 (1990) 2229.
[21] M. Cattaneo, F. Fagalde, N.E. Katz, C.D. Borsarelli, T. Parella, Eur. J. Inorg. Chem. (2007) 5323.
[22] J. Otsuki, N. Omokawa, K. Yoshiba, I. Yoshikawa, T. Akasaka, T. Suenobu, T. Takido, K. Araki, S. Fukuzumi, Inorg. Chem. 42 (2003) 3057.
[23] W. Kaim, Coord. Chem. Rev. 463 (2001) 219.
[24] J.L. Sadler, A.J. Bard, J. Am. Chem. Soc. 90 (1968) 1979.
[25] K.C. Gordon, A.H. Flood, S.M. Scott, S.L. Howell, J. Phys. Chem. A 109 (2005) 3745.
[26] D.M. Dattelbaum, K.M. Omberg, J.R. Schoonover, R.L. Martin, T.J. Meyer, Inorg. Chem. 41 (2002) 6071.
[27] A.H. Gemeay, Dyes Pigm.. 54 (2002) 201.
[28] A.I. Baba, J.R. Shaw, P.A. Simon, R.P. Thummel, R.H. Schmehl, Coord. Chem. Rev. 171 (1998) 43.
[29] J. Otsuki, M. Tsujino, T. Iizaki, K. Araki, M. Seno, K. Takatera, T. Watanabe, J. Am. Chem. Soc. 119 (1997) 7895.
[30] M. Arias, J. Concepción, I. Crivelli, A. Delgadillo, R. Díaz, M.A. Francois, F. Gajardo, R. López, A.M. Leiva, B. Loeb, Chem. Phys. 326 (2006) 54.
[31] D. Sundholm, S. Taubert, F. Pichietti, PCCP 12 (2010) 2751.